Coupling between plasticity and phase transition in single crystal iron at ultra-high strain rate

Cite as: AIP Conference Proceedings **2272**, 070001 (2020); https://doi.org/10.1063/12.0001011
Published Online: 04 November 2020

N. Amadou, T. de Rességuier and A. Dragon

Coupling Between Plasticity and Phase Transition in Single Crystal Iron at Ultra-High Strain Rate

N. Amadou,[1, a)] T. de Rességuier[2] and A. Dragon[2]

[1] *Département de Physique, Université Abdou Moumouni de Niamey, BP. 10662 Niamey, Niger.*
[2]*Institut P'. CNRS. ENSMA. Université de Poitiers, Poitiers, France.*

[a)] *Corresponding author: nourou.amadou@polytechnique.edu*

Abstract. Solid materials behavior under ultra-high strain rate loading such as shock compression may involve various processes including plastic deformation, structural phase transformations, fracture, melting, etc., whose kinetics and coupling are complex functions of strain rate, initial conditions and microstructure. Here, we present molecular dynamics simulations of the dynamic response of single-crystal iron to either ramp or shock compression, at strain rates on the order of 10^9 s^{-1}, where we focus on the coupling between plastic deformation and the bcc-hcp phase transition. Defect-free crystal at 50 K initial temperature was found to yield via twinning when compressed along the [001] direction. Then, the onset of the bcc-hcp transformation was shown to be tightly dependent on the plasticity history through a shear-stiffening effect, which in some conditions inhibits the nucleation of the hcp phase [N. Amadou et al., Phys. Rev. B **98**, 024104, 2018]. Yet, changing the direction of load application versus crystal orientation, or introducing lattice defects lead to very different behavior, including dislocation-mediated plasticity.

INTRODUCTION

Understanding the properties of materials at ultra-high strain rates (greater than 10^6 s^{-1}) constitutes an issue of considerable interest for both materials science and shock physics communities [1-3]. Indeed, under such conditions, ordinary solid-state deformation processes such as plastic flow and phase transformation operate far from equilibrium and show important kinetic effects [4], which could result in an exotic response.

In practice, to achieve such ultra-high strain rate, a dynamic compression is used where the simplest way is to generate a shock wave in the sample [5]. However, shock loading is a highly dissipative process, which causes an entropy jump and high temperatures so that materials may melt. In order to preserve the solid state, the so-called "quasi-isentropic" ramp compression, where the pressure pulse is shaped to rise more progressively over time, is alternatively used [1].

Perhaps the most widely studied material under dynamic compression is iron due to its industrial and fundamental (mainly in geophysics) importance. It is well established, from earlier shock compression experiments (strain typically less than 10^6 s^{-1}), that iron undergoes both plastic deformation and structural phase transition from the ground-state body-centered cubic (bcc) structure (α phase) to the high-pressure hexagonal close packed (hcp) structure around pressures of 1 and 13 GPa, respectively [6,7].

However, at high strain rates, depending on the compression time scale and sample initial conditions, iron may exhibit plasticity [6,7] or not [8,9] before the structural bcc-hpc phase transition. Besides, the bcc-hcp transition onset pressure is shown to vary from 11 to 34 GPa [8-11]. On the other hand, on the theoretical side the situation is hardly simpler. Indeed, depending on the interatomic potential model used, iron is found to remain perfectly elastic [12] or undergo dislocation-based plastic deformation [13,14] before the phase transition. Here, the transition onset pressure varies from 15 to 39 GPa [12-15]. Thus, under ultra-high strain rate, plasticity, phase transition, their kinetics, and their coupling still remain open issues.

In a recent paper [16], we reported molecular dynamics simulations showing the coupling between plasticity and phase transition in [001]-oriented single crystal iron dynamically compressed at strain rates of about 10^9 s^{-1}. Under

Shock Compression of Condensed Matter - 2019
AIP Conf. Proc. 2272, 070001-1–070001-6; https://doi.org/10.1063/12.0001011
Published by AIP Publishing. 978-0-7354-4000-5/$30.00

both shock and ramp compression, iron was found to yield via twinning. While shock compression above the yield strength was found to trigger the bcc-hcp transition in the expected pressure range, a "shear-stiffening" process was observed under ramp compression, resulting in a transient inhibition of the phase transformation up to much higher onset pressures. Here, we first recall those observations, then we extend our investigation to other low crystallographic index, by loading the single crystal along its [110] and [111] orientations, and we explore the influence of initial defects. Very different responses are evidenced, including dislocation-dominated plasticity.

COMPUTATIONAL DETAILS

In order to study the coupling between plasticity and phase transition at ultra-high strain rate, non-equilibrium molecular dynamic simulations were realized using the Lammps code [17]. Samples of up to 50 millions of atoms equilibrated at initial temperature of 50 K, either defect-free or defective, were simulated using the formalism of the embedded atom model to handle the interactions between atoms [18]. The iron model is the recently modified version of the Ackland potential [19], which accounts for both plasticity and phase transformation [13,19]. In the defective sample case, the defects are introduced in the form of micro-voids of $5a_0$-radius (with a_0 the lattice constant) regularly spaced by $100a_0$ along the wave propagation direction.

Either shock or ramp wave are initiated by driving an effective infinite-mass wall piston with an imposed velocity $v(t)$ along the z-direction, while periodic boundary conditions are applied in the transverse directions. The compression wave propagates along the [001], [110] and [111] directions respectively. The piston velocity increases linearly from 0 to V_{max} within 15 or 30 ps, with V_{max} ranging from 800 to 1600 m/s. The corresponding strain rates are about 10^8 - 10^9 s^{-1} comparable with that reported under picosecond-laser dynamic compression [20].

Local thermodynamic and mechanical variables such as longitudinal pressure P_z, deviatoric stress, temperature, etc. are evaluated within a spatial planar bin (of 3 lattice constant width) perpendicular to the wave propagation direction (see ref. [16] for details). Finally, local structural analysis is performed by adaptative Common Neighbor Analysis (CNA), Centro-symmetry and DXA, as implemented in the OVITO software [21].

RESULTS

Shock compression

Beyond a certain amplitude, a compression front propagating trough iron is expected to split into three waves: an elastic precursor associated with elastic compression of the bcc phase, a plastic wave carrying bcc iron up to the bcc-hcp phase boundary (sometimes referred to as the P1 wave), and a slower transformation wave in which the bcc to hcp transition proceeds (sometimes referred to as the P2) [6,7]. These wave profiles coupled with an in situ analysis of the sample lead to valuable information on the deformation process, specifically on the micro-process underling plasticity and phase transition at atomic level and their characteristic time scales.

Fig. 1 (a) shows snapshots of atoms configuration at two simulations times respectively, where the sample is shock compressed to piston maximum velocity of 800 m/s corresponding to P_z of about 48 GPa. The corresponding wave profiles are presented in Fig. 2 (b). Here, the elastic wave is overdriven by the P1 wave, so that only the P1 and P2 waves are observed. The defects associated with plastic compression are identified to be twins (see Fig. 1 (c)) in consistence with previous MD simulations of plastic deformation in bcc material such as tantalum [22] and with the dynamic behavior of iron observed under both impact [23,24] and laser shock loading [25]. However it contrasts with an absence of plasticity reported in other experiments [8,9,26] as well as in MD simulations that used the Voter–Chen potential [12], and with dislocation-based plasticity observed in polycrystalline iron in other MD simulations [13,14]. The pressure P_z of about 29 GPa at the top of the P1 wave corresponds to the onset pressure of the structural phase transformation. Although this value is greater than that the 13 GPa value at equilibrium conditions [6,7], it is consistent with what was found under dynamic laser compression [9-11] and with MD simulations of polycrystals [13].

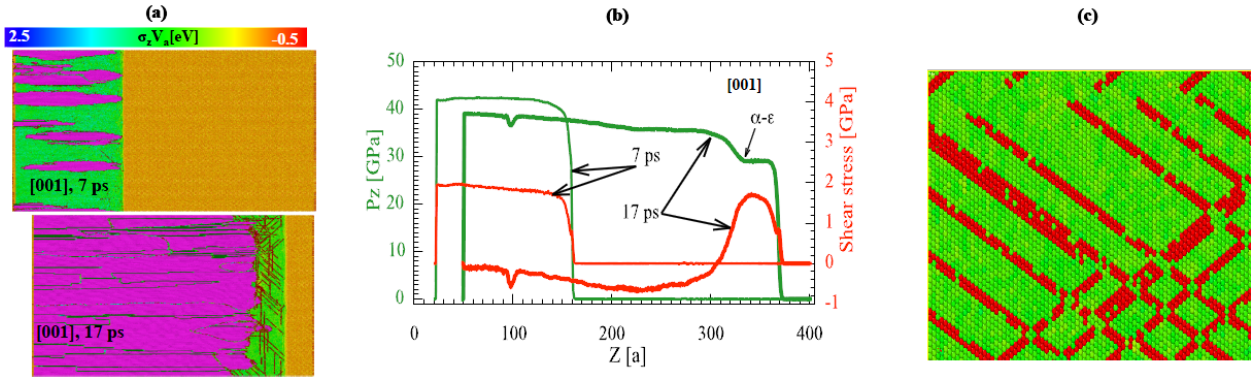

FIGURE 1: (a) Atomic structure snapshots at two different simulation time steps. The non hcp and fcc atoms are colored according to Pz (i.e. the z-component of the atomic stress σ times the atomic volume V_a), except for atoms in twins, which are colored in brown. Violet and dark-green are the hcp and fcc atoms respectively. (b) Corresponding wave profiles with green curves depict longitudinal pressure Pz while red curves present shear stress. (c) Example of atom configuration in the $(1\bar{1}0)$ plane under dynamic compression to P_z of 19. Redcolored atoms are associated with twins.

Ramp compression

When ramp-compressed, the [001]-oriented defect-free iron single crystal response is quite different from under shock compression. Fig. 2 shows atomic configuration snapshot (a), longitudinal pressure P_z (b) and shear stress (c) at different simulations times, where the sample was ramp compressed to piston maximum velocity of 1600 m/s over 30 ps. The corresponding maximum pressure P_z is about 140 GPa.

Here, the sample is first elastically compressed up to about 12 GPa then yields via twinning, which relaxes the shear stress as in the case of shock compression. However, in contrast to the shock compression case, on further compression, when pressure P_z reaches about 18 GPa, the twins start to recede while no dislocation activities are detected (see blue zone in Fig. 2 (a) at 25 and 33 ps), leading to a new increase of the shear stress to values as high as 30 GPa (Fig. 2 (c)). Such elastic stiffening of the bcc matrix inhibits the nucleation of the hcp phase, so that the onset of the phase transformation in the defect-free crystal is shifted to very high pressures. Thus, for the transition to be observed a pressure as high as 100 GPa is required (see [16] for more details) which has been qualitatively explained by invoking phase nucleation and growth theory [27].

On the other hand, when defects are introduced in sample in the form of microvoids, the onset pressure of the bcc to hcp phase transition decreases to a value around 28 GPa [28]. Indeed, when P_z locally reaches a value of about 17 GPa, an emission of dislocations, mainly of screw type, from microvoids is observed in consistence with that reported for other bcc materials such as tantalum [29]. Even though the growth of these dislocations is found to be very slow for this loading direction, their contribution is found to be sufficient to trigger the structural phase transition near defects where the work required for nucleation is much reduced [27]. This observation illustrates the importance of defects in the development of martensitic phase transformations.

When ramp-compressed along the [110] crystallographic direction, defect-free single crystal iron exhibits a complex deformation behavior. Indeed, the sample remains perfectly elastic, with the shear stress linearly increasing, until the pressure reaches about 27 GPa. A first yielding then occurs via simultaneous nucleation of twins and hcp phase (only few fcc atoms are observed at this stage) (Fig. 3 (a) top). Upon further compression the shear stress increases again with hcp atoms fraction remaining almost constant (Fig. 3 (b), thin curves). Thus a mixed phase regime is observed where dislocations develop when the pressure P_z reaches about 40 GPa (Fig. 3 (c)). The dislocations growth is accompanied by increasing number of fcc atoms while the number of hcp atoms decreases slightly until the shear stress attains 10 GPa. Only then, the hcp rapid growth regime is found to be triggered thus leading the structural phase transformation toward completion. With defective initial conditions, the dislocations are found to start near microvoids when the pressure P_z reaches about 20 GPa. They are followed by twinning and hcp phase nucleation at P_z of 22 GPa.

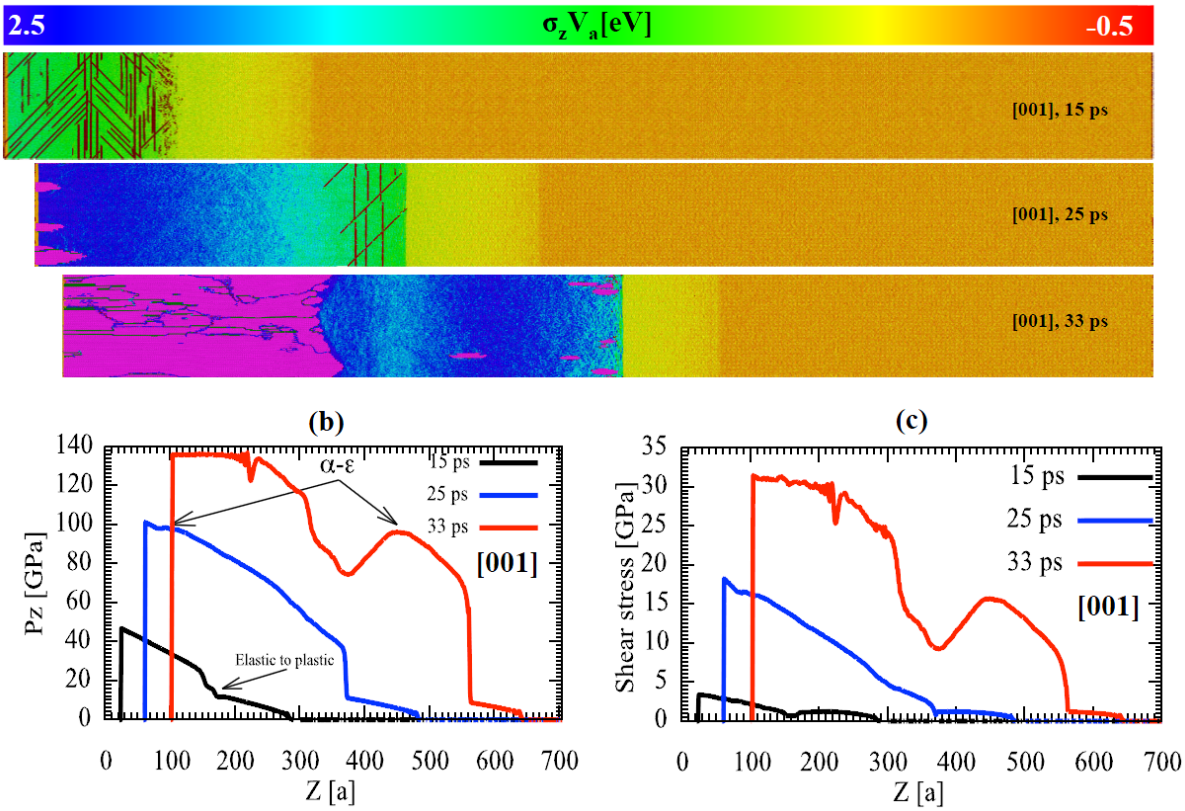

FIGURE 2: (a) Atomic structure snapshots at 15, 25 and 33 ps simulation times for [001]-oriented defect-free single crystal iron ramp-compressed to piston maximum velocity of 1600 m.s^{-1} (corresponding to maximum P_z of about 140 GPa) within 30 ps. Atoms color codes are the same as in Fig. 1 (a). Corresponding profiles of longitudinal pressure P_z (b) and shear stress (c).

Finally, along the [111] loading direction, iron single crystal is found to remain perfectly elastic until the onset of the bcc to hcp phase transition, at pressure P_z about 35 GPa, (Fig 3. (a) bottom and Fig. 3 (b) thick curves) which is found to be the preferential way to relax shear stress upon compression. Thus, no plastic deformation is detected before the phase transformation in consistence with previous MD simulations of the iron single crystal response to both shock compression [12] and non-equilibrium uniaxial deformation [30] along [111] direction. However, with defective initial condition, [111]-oriented crystal yields via dislocations emission from microvoids when the pressure P_z reaches about 20 GPa, then the phase transition occurs at about 33 GPa [28].

CONCLUSIONS

We have studied the coupling between plasticity and phase transition in single crystal iron at ultra-high strain rate of about 10^9 s^{-1} using molecular dynamic simulations. Defect-free crystal at 50 K initial temperature is found to yield via twinning when both shock and ramp compressed along the [001] direction. Under shock compression the bcc to hcp phase transition is shown to occur around 29 GPa in consistence with the literature. However, under ramp compression, yielding is followed by elastic stiffening that shifts the bcc to hcp phase transition to high pressure of about 100 GPa. When initial defects are introduced in the sample in the form of microvoids, a transition onset pressure of about 28 GPa is evidenced, illustrating the importance of defects in the development of martensitic phase transformations. Besides, ramp compression along other crystal orientations leads to very different responses. While perfect crystals compressed in the [111] direction remain basically elastic up to the onset of the phase transition (around 35 GPa), those compressed in their [110] direction exhibit a complex behavior, with simultaneous twinning and massive nucleation of hcp phase (at about 27 GPa) creating a mixed-phase, metastable regime where dislocations develop (above about 40 GPa). With defective initial conditions, both [110] and [111]-oriented crystals exhibit plastic deformation mainly dominated by dislocations.

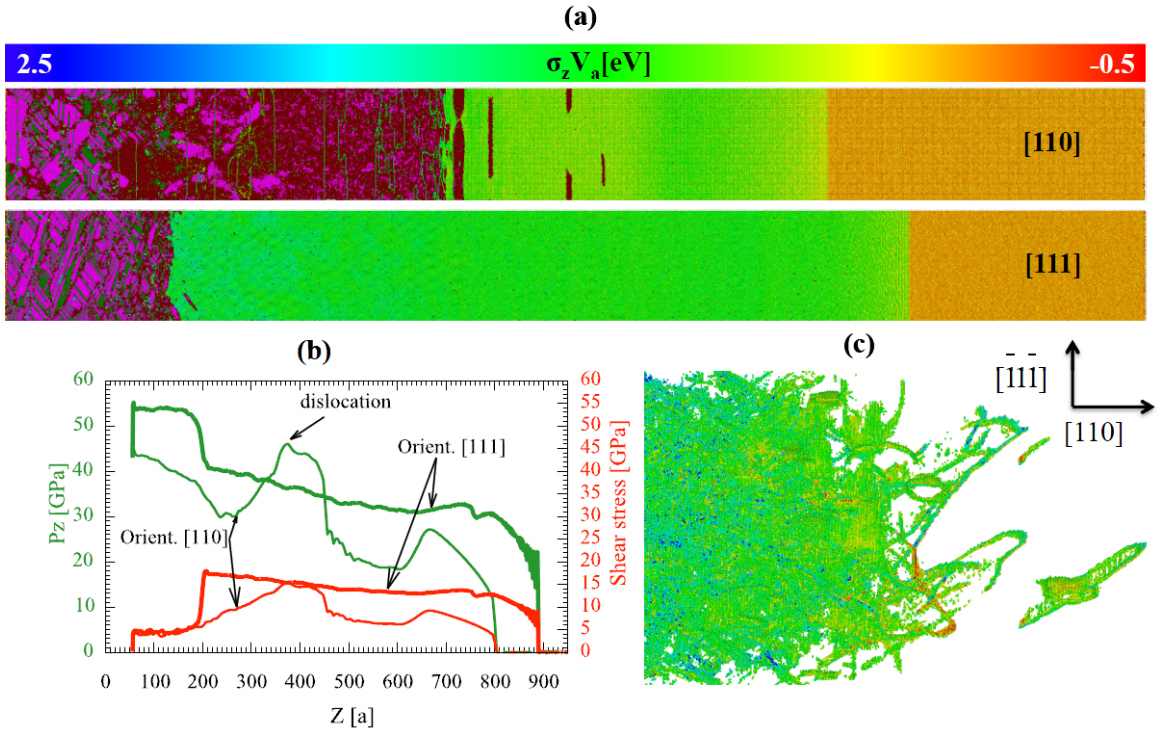

FIGURE 3: (a) Atomic structure snapshots at 40 ps simulation time-step for [110] (top row) and [111] (bottom row) directions in defect-free iron single crystal iron, ramp compressed to piston maximum velocity of 800 m.s^{-1} (corresponding to maximum Pz of about 50 GPa) within 30 ps. Atoms color codes are the same as in fig. 1 (a). (b) corresponding wave profiles with thin and thick curves corresponding to [110] and [111] directions respectively. The green curves depict longitudinal pressure Pz while red curves present shear stress. (c) Extract of the mixed regime from fig. 3 (top) showing particles with unknown coordination structure (by CNA analysis) showing dislocation loops in the mixed phase regime, in [110]-oriented defect-free.

ACKNOWLEDGMENTS

Computations were run on the supercomputer facilities of the *Mésocentre de calcul de Poitou-Charentes* (France).

REFERENCES

1. B. A. Remington, G. Bazan, J. Belak et al, *Metall. Mater. Trans. A* **35**, 2587 (2004)
2. B. A. Remington, P. Allen, E. M. Bringa et al, *Materials Science and Technology.* **22**, 474 (2006)
3. B. A. Remington, R. E. Rudd, and J. S. Wark, *Physics of Plasmas*, **22**, 090501, (2015)
4. R. E. Rudd, T. C. Germann, B. A. Remington and J. S. Wark, *MRS Bulletin* **35,** 999 (2010)
5. Y. B. Zel'dovich and Y. P. Raizer, *Physics of shock waves and high-temperature hydrodynamic phenomena* (Dover publication, New York, 2002), pp. 685-784
6. L. M. Barker and R. E. Hollenbach, *J. Appl. Phys*. **45**, 4872 (1974)
7. J. C. Boettger and D. C. Wallace, *Phys. Rev. B*, **55**, 2840-2849 (1997)
8. D. H. Kalantar, J. F. Belak, G. W. Collins et al, *Phys. Rev. Lett*. **95**, 075502 (2005)
9. N. Amadou, T. de Resseguier, E. Brambrink, et al, *Phys. Rev. B*. **93**, 214108 (2016)
10. N.Amadou, E. Brambrink,T. de Rességuier et al., *Metals* **6**, 320 (2016)
11. R. F. Smith, J. H. Eggert, D. C. Swift et al, *J. Appl. Phys*. **114**, 223507 (2013)
12. K. Kadau, T. C. Germann, P. S. Lomdahl, and B. L. Holian, *Phys. Rev. B* **72**, 064120 (2005)
13. N. Gunkelmann, E. M. Bringa, D. R. Tramontina et al, *Phys. Rev. B* **89**, 140102 (2014)
14. K.Wang, S. Xiao, H. Deng,W. Zhu, and W. Hu, *Int. J. Plast*. **59**, 180 (2014)
15. H.-T. Luu and Nina Gunkelmann, *Computational Materials Science* **162**, 295–303 (2019)
16. N. Amadou, T. de Resseguier, A. Dragon and E. Brambrink, *Phys. Rev. B*. **98**, 024104 (2018)
17. S. Plimpton, J. Comp. Phys. **117**, 1–19, (1995)

18. M. S. Daw and M. I. Baskes, *Phys. Rev. Lett*., **50**, 1285–1288 (1983)
19. N. Gunkelmann, E. M. Bringa, K. Kang, G. J. Ackland et al., *Phys. Rev. B*, **86**, 144111 (2012)
20. J. C. Crowhurst, B. W. Reed, M. R. Armstrong et al., *J. Appl. Phys*., **115**, 113506 (2014)
21. A. Stukowski, Modelling and Simulation in Materials Science and Engineering, **18**, 015012, (2009)
22. R. Ravelo, T. C. Germann, O. Guerrero, Q. An, and B. L. Holian, *Phys. Rev. B* **88**, 134101 (2013)
23. J. N. Johnson and R.W. Rohde, *J. Appl. Phys*. **42**, 4171 (1971)
24. M. A. Meyers and L. E. Murr, *Shock Waves and High-Strain-Rate Phenomena in Metals* (Plenum, New York, 1980), p. 487
25. T. de Rességuier and M. Hallouin, *J. Appl. Phys*. **84**, 1932 (1998)
26. J. Hawreliak, J. D. Colvin, J. H. Eggert et al., , *Phys. Rev. B* **74**, 184107 (2006)
27. J.W. Christian, *The Theory of Transformations in Metals and Alloys* (Elsevier, 2002). pp 422-479
28. N. Amadou, T. de Resseguier, A. Dragon and E. Brambrink, *to be published*
29. C.J. Ruestes, E.M. Bringa, A. Stukowski et al., *Comput. Mater. Sci*., **88**, 92 – 102 (2014)
30. B. T. Wang, J. L. Shao, G. C. Zhang et al., *Journal of Physics: Condensed Matter*, **21,** 495702 (2009)